J. Phys. B: At. Mol. Opt. Phys. 28 (1995) 2221–2231. Printed in the UK

Velocity and core-electron effects in state-selective electron capture following Ar^{8+}–Li collisions

E Jacquet†‡, J Pascale§, P Boduch†‡, M Chantepie†‡ and D Lecler†

† Laboratoire de Spectroscopie Atomique, CNRS-ERS 137, ISMRA, 6 Boulevard Maréchal Juin, F-14050 Caen Cedex, France

‡ UFR des Sciences, Université de Caen, F-14032 Caen Cedex, France

§ Service des Photons, Atomes et Molécules, Centre d'Etudes de Saclay, CEA, Bâtiment 522, F-91191 Gif sur Yvette Cedex, France

Received 29 November 1994, in final form 23 March 1995

Abstract. The effect of the velocity of the incident ions in the *nl*-distributions of the electron capture in collisions of highly charged Ar^{8+} ions with a lithium target is studied. These Ar^{8+}–Li(2s) collisions are experimentally studied by means of near UV and visible photon spectroscopy (200–600 nm) in the 1.5–4.5 keV amu^{-1} energy range and theoretically analysed by means of the three-body classical trajectory Monte-Carlo method. The presence of projectile core-electrons strongly affects the population and collision energy dependence of low l values produced in the electron capture reaction. It is shown that the $\sigma(nl)$ partial cross sections ($n = 8$, 9 and $l = 0$, 1, 2) increase with decreasing energies.

1. Introduction

We have recently studied single electron capture in 120 keV X^{8+}–Li(2s) collisions (X ≡ Ar, Kr) by means of near UV and visible photon spectroscopy and have performed three-body classical trajectory Monte-Carlo (CTMC) calculations for these collisions and also for Ne^{8+} and O^{8+}–Li(2s) collisions (Jacquet *et al* 1993, 1994, Jacquet and Pascale 1995). The experimental $\sigma(nl)$ cross sections for capture into the *nl* sublevels of X^{7+} were found to be, for the most populated $n = 8$ and $n = 9$ levels, in fair agreement with the CTMC results. As previously observed in collisions with fully stripped ions, i.e. C^{6+}, O^{8+}–Li collisions (Olson *et al* 1992), it was found that states with large l values are predominantly populated but, in the case of Ar^{8+}–Li and Kr^{8+}–Li collisions, states with low l values ($l \leqslant 3$) are also populated (cf table 1). This result was attributed to a core-electron effect, already predicted by CTMC calculations for N^{5+} and Ar^{8+}–Cs(6s) collisions (Pascale *et al* 1990). In the case of 160 keV Ar^{8+}–Cs(6s) collisions, the cross sections were found to be in good agreement with the CTMC results (Martin *et al* 1992, Denis *et al* 1994). For Ne^{8+} and Ar^{8+}–Na(3s) systems, the cross sections for low l-subshells of $n = 9$ states were found to dominate (Gauntt and Danzmann 1992). This effect was found to be more important in the case of Kr^{8+}–Li collisions than in the case of Ar^{8+}–Li collisions.

Following Harel and Jouin (1988) who have made an extensive study of the single electron capture in X^{8+}–H(1s) collisions (X ≡ O, Ne, Ar) for the 1–16 keV amu^{-1} energy range using a semi-classical close-coupling method, these very non-statistical *nl*-distributions were explained as the result of the competition between two mechanisms: the Stark effect due to the residual ion (Li^+ or H^+) and the projectile core-electron effect. The Stark effect mixes states of degenerate or nearly degenerate *nl* sublevels, the population

0953-4075/95/112221+11$19.50

Table 1. CTMC calculated cross sections (10^{-16} cm^2) for single electron capture into the $8l$ and $9l$ sublevels in 3 keV amu^{-1} X^{8+}–Li collisions (X ≡ O, Ne, Ar, Kr).

Projectile *nl*	O^{8+}	Ne^{8+}	Ar^{8+}	Kr^{8+}
8s	0.43	2.24	14.34	4.43
8p	1.77	2.48	18.69	11.83
8d	4.37	4.23	7.42	32.55
8f	10.55	9.72	4.12	21.86
8g	19.71	18.51	11.35	6.11
8h	32.77	30.31	21.65	14.35
8i	42.27	43.63	37.03	27.37
8k	54.27	53.86	50.25	46.71
total	166.14	164.97	164.84	165.22
9s	0.24	0.98	5.37	10.96
9p	1.19	1.24	6.46	20.44
9d	2.39	1.93	4.92	30.62
9f	5.82	5.53	4.36	13.02
9g	9.96	11.06	11.24	5.94
9h	23.52	21.46	19.81	15.31
9i	43.21	43.63	36.48	27.60
9k	63.21	61.61	57.98	49.46
9l	70.36	69.46	67.81	59.13
total	219.90	216.89	214.44	231.47

of states with large l values is then favoured. In the case of fully stripped ions (O^{8+}) or nearly fully stripped ions (Ne^{8+}), all the nl sublevels are, for a given n, degenerate or almost degenerate and then only states with large l values are populated by single electron capture. In the case of Ar^{8+} and Kr^{8+} ions, the states with low angular momenta ($l = 0$–3) are not degenerate, then, the Stark effect mixes only states with large angular momenta which are quasi-degenerate. The core-electron effect results from contributions of avoided crossings between adiabatic potential energy curves which are correlated asymptotically to the entrance channel and to the various outgoing channels. The avoided crossings are adiabatic for curves corresponding to states with low angular momenta so that states with low l values are populated by the core-electron effect. In the case of X^{8+}–H(1s) collisions, the projectile core-electron effect is more important for Ar^{8+} than for Ne^{8+} because of avoided crossings with larger energy splittings in the case of Ar^{8+}.

The projectile core-electron effect is more important for Kr^{8+} than for Ar^{8+}, then, the cross sections for nl sublevels ($l \leqslant 3$) are more important in the case of Kr^{8+}–Li collisions than in the case of Ar^{8+}–Li collisions. Recently, CTMC calculations for the single electron capture for Kr^{8+}–Li collisions have shown that final nl-distributions depend strongly on the energy of the incident ions in the 1.4–15 keV amu^{-1} energy range (Jacquet *et al* 1994). In the case of Ar^{8+}–Cs(6s) collisions, at 16 keV, the $\sigma(nl)$ partial cross sections with low l values are larger than the $\sigma(nl)$ with large l values, while at 160 keV, only high l levels were found to be significantly populated (Denis *et al* 1994). The core-electron effect is negligible at high energies and increases with decreasing energies. In order to confirm these predictions, we have experimentally studied Ar^{8+}–Li collisions for incident energies between 1.5 keV amu^{-1} and 4.5 keV amu^{-1}. Because of technical reasons, we could not study Kr^{8+}–Li collisions in this energy range.

We report the experimental results of the energy dependence of the projectile core-electron effect together with the corresponding CTMC results. The Ar^{8+}–Li collisions are studied by means of near UV and visible photon spectroscopy, the experimental set-up and

the spectroscopic analysis method will be briefly described. The obtained cross sections will be presented and compared with those calculated by using the three-body CTMC method.

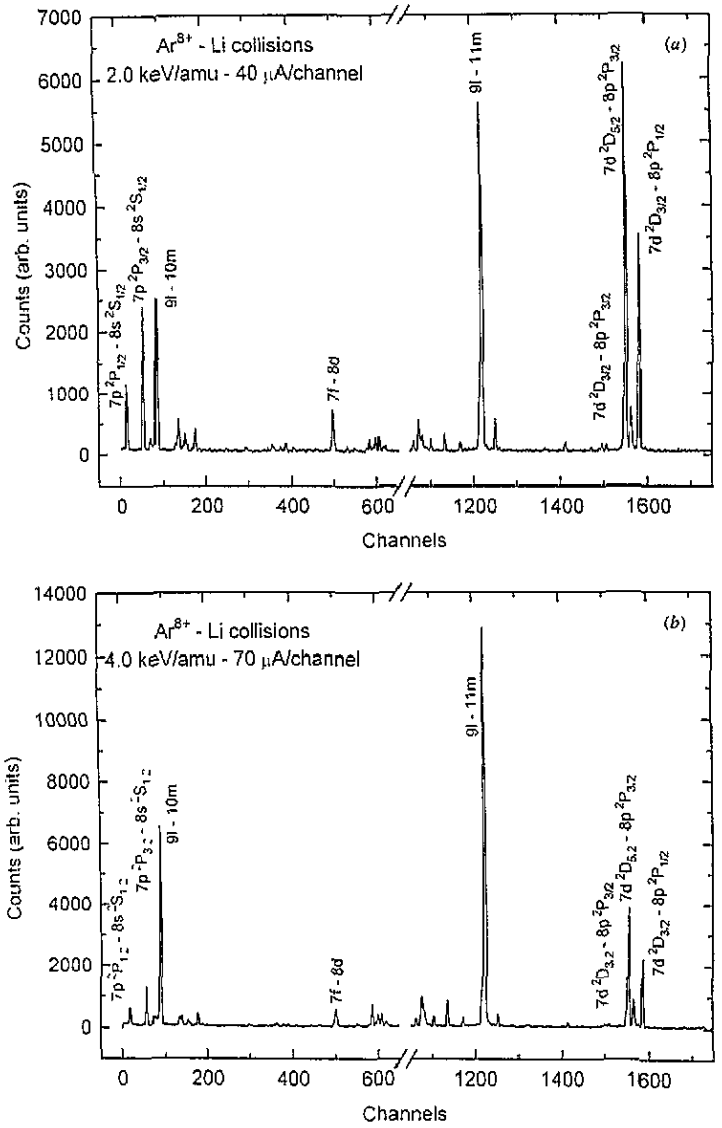

Figure 1. Spectra of Ar^{8+}–Li collisions. (a) Projectile energy of 2.0 keV amu^{-1}, 40 μA/channel. (b) Projectile energy of 4.0 keV amu^{-1}, 70 μA/channel.

2. Experimental set-up

An argon beam produced by an ECR source of the GANIL† test bench was charge and mass analysed to obtain a pure Ar^{8+} ion beam. The beam current was of the order of

† Grand Accélérateur National d'Ions Lourds, Caen, France.

25 μA with an energy of 7.5 $q$keV, i.e. 60 keV and 80 μA with an energy of 22.5 $q$keV, i.e. 180 keV. The incident beam was focused on an effusive jet of lithium atoms inside a collision chamber. The lithium atoms are in their ground state, their electronic structure is then $1s^2 2s$. The photons emitted at right angles to the directions of the incident ion beam and of the lithium jet were focused on the entrance slit of a normal incidence grating spectrometer of 700 mm focal length (Sopra 700) equipped with a 1200 grooves/mm grating blazed for 750 nm in the first order and were detected in the 200–600 nm wavelength range with a photomultiplier (Hamamatsu R106). An example of a spectrum is presented for two energies (figures 1(a) and (b)). It is typical of velocity effects. The spectral analysis of such emissions has already been presented in detail (Jacquet *et al* 1993).

Emission cross sections were determined for each transition using the absolute calibration of the line intensities and the spectroscopic response of the optical device. The absolute calibration of the line intensities has been obtained by recording the spectra for 60 keV C^{4+}–Li collisions and by using the excitation cross sections for $C^{3+}(nl)$ measured by Dijkkamp *et al* (1984). The response of our detection system takes into account the theoretical grating efficiency and the phototube response given by the manufacturer. This theoretical response is then fitted with well known lines of C IV.

3. Experimental results

The classical over-barrier model (Niehaus 1986) predicts that, for typical Ar^{8+}–Li collisions, the 2s electron of the lithium atom is predominantly captured into the $n = 8$ and $n = 9$ levels. The experimental emission cross sections of all the observed lines are given in table 2 for projectile energies between 1.5 keV amu^{-1} and 4.5 keV amu^{-1}. If a group of lines (7h–8i, 7i–8k), (8i–9k, 8k–9l) was not sufficiently resolved, the individual emission cross sections were deduced from the emission cross sections of the unresolved structure and from relative intensity measurements performed with narrower spectrometer slits.

The uncertainties of the experimental emission cross sections are due to the calibration method and to the polarization of the light by the grating. As the Ar^{8+} ion beam and the lithium jet are stable, the uncertainties due to the calibration depend mainly on the uncertainties of the cross sections given by Dijkkamp *et al* (1984). The uncertainties due to polarization effects are difficult to evaluate: they depend on the wavelengths, on the diffraction order and on the polarization of the detected lines. If we assume that the polarization rates of the C^{3+} and Ar^{7+} lines are of the same order—that is probably the case for the strongest lines (yrast lines)—these uncertainties are probably small. We suppose that an upper limit of 30% for the relative uncertainties is large enough to take into account the most important error sources.

The cross sections for single electron capture into the $8l$ and $9l$ sublevels (i.e. for the most populated $n = 8$ and $n = 9$ states) were deduced from emission cross sections and transition probabilities (Lindgard and Nielsen 1977). These experimental cross sections are presented in table 3. The uncertainties are estimated to be lower than $\pm 40\%$ in order to take into account the uncertainties due to the method. Such a limit is probably good for the strongest lines (yrast or near yrast lines) which have large branching ratios but perhaps a little bit specious for lines having small branching ratios.

4. Comparisons with the CTMC calculated cross sections

The CTMC method used in the calculations is based on solving the Hamilton's equations for the motion of a three-body system (the valence electron, the alkali metal core (Li^+) and

Table 2. Experimental emission cross sections (10^{-16} cm^2) versus the projectile energy (keV amu^{-1}) for single electron capture following Ar^{8+}–Li collisions. The experimental uncertainties are always lower than ±30%.

Energy / Transition	1.5	2.0	2.5	3.0	3.5	4.0	4.5
7p–8s	3.1	2.3	1.7	1.4	1.2	0.77	0.61
7d–8p	1.9	1.8	1.3	1.1	0.98	0.77	0.71
7d–8f	0.25	0.21	0.19	0.23	0.20	0.18	0.18
7f–8d	0.18	0.17	0.14	0.12	0.10	0.10	0.09
7f–8g	1.8	2.2	2.2	2.3	2.6	2.3	2.6
7g–8h	9.3	10.5	11.2	11.1	12.3	11.3	12.4
7h–8i	34.8	39.4	41.9	41.5	46.1	42.2	46.3
7i–8k	104.4	118.3	125.8	124.6	138.4	126.7	139.0
8p–9s	2.1	1.4	0.92	0.37	0.33	0.24	0.17
8d–9p	0.69	0.48	0.40	0.34	0.28	0.20	0.19
8d–9f	0.10	0.09	0.06	0.06	0.05	0.05	0.05
8f–9g	0.64	1.6	1.3	0.99	1.4	1.2	0.72
8g–9h	3.7	4.4	4.8	3.9	5.8	5.3	5.7
8h–9i	8.3	10.9	12.6	10.6	13.3	17.0	12.8
8i–9k	21.2	28.8	35.1	29.9	37.2	45.3	32.5
8k–9l	46.2	62.5	78.4	59.7	67.2	76.0	70.8
4d–4f	0.12	0.12	0.15	0.15	0.18	0.17	0.17
9h–10i	0.55	1.1	1.0	1.6	1.6	1.9	1.7
9i–10k	1.0	1.9	2.1	3.5	4.0	4.5	3.2
9k–10l	2.3	3.9	4.5	7.3	7.9	7.7	7.2
9l–10m	4.0	7.3	7.9	11.3	10.6	10.4	12.7
8g–10h	0.16	0.23	0.20	0.37	0.29	0.25	0.32
8h–10i	0.38	0.44	0.44	0.88	0.76	0.76	0.76
8i–10k	0.64	0.60	0.72	1.5	1.5	1.4	1.3
8k–10l	0.82	0.74	0.93	1.9	1.8	1.5	1.7
9h–11i	0.21	0.20	0.24	0.29	0.22	0.23	0.19
9i–11k	0.35	0.24	0.41	0.44	0.38	0.31	0.32
9k–11l	0.56	0.27	0.50	0.58	0.62	0.49	0.52
9l–11m	0.61	0.30	0.41	0.57	0.66	0.56	0.55

the ionic core projectile) given a set of initial conditions for the projectile and the target (Abrines and Percival 1966, Olson and Salop 1977). Details of the CTMC method which uses effective electron–core interactions and the method of Reinhold and Falcon (1986) for the initialization of the target electron are given by Pascale *et al* (1990) and Olson *et al* (1992). Model potentials have been used to describe the interactions between the active electron and the two ionic cores. For the e^-–Li^+ interaction, we have used (Klapisch 1967):

$$V_{Li}(r) = -\frac{1}{r}\left[1 + 2e^{-7.9r} + 10.31re^{-3.848r}\right]$$

and for e^-–Ar^{8+} interaction we have (Pascale *et al* 1990):

$$V_{Ar^{7+}} = -\frac{1}{r}\left[8 + 10(1 - 1.706r + 1.039r^2)e^{-3.5r}\right]$$

These model parameters have the correct behaviour at large and small values of r, and the parameters of the functional form of the potentials were determined to fit spectroscopic data (Jacquet *et al* 1994).

Table 3. Experimental cross sections (in 10^{-16} cm^2) versus the projectile energy (keV amu^{-1}) for single electron capture into the $8l$ and $9l$ sublevels for Ar^{8+}–Li collisions. The experimental uncertainties are always lower than ±40%.

Energy *nl*	1.5	2.0	2.5	3.0	3.5	4.0	4.5
8s	29	21	16	13	11	7.1	5.7
8p	23	23	15	14	12	9.8	9.1
8d	6.5	6.4	5.1	4.4	3.5	3.6	3.6
8f	6.1	4.0	3.9	5.4	4.1	3.7	4.1
8g	8.4	11	10	11	12	10	12
8h	22	24	25	27	27	20	28
8i	40	41	39	42	43	28	49
8k	57	55	47	63	60	49	67
total	192	185	161	179	182	131	179
9s	27	17	12	4.6	4.1	3.0	2.1
9p	12	8.1	6.7	5.7	4.7	3.4	3.2
9d	2.6	3.8	3.2	3.5	4.0	3.1	3.6
9f	4.1	3.6	2.6	2.5	2.2	2.2	1.9
9g	6.7	17	14	10	14	13	7.6
9h	19	22	24	18	29	26	28
9i	23	30	35	27	35	45	34
9k	32	43	53	42	53	67	46
9l	42	55	70	48	56	65	58
total	168	200	220	161	202	228	184

We have considered the asymptotic quantum defects $\delta(l)$ of the Ar^{7+} ions (Theodosiou *et al* 1986) for analysing the final nl-distributions: $\delta(0) = 0.5245$, $\delta(1) = 0.3611$, $\delta(2) = 0.1183$, $\delta(3) = 0.0096$ and $\delta(l \geqslant 4) = 0$. For each trajectory ending with the electron capture process, the final nl-sublevel is determined from the following procedure:

First, from the calculated classical angular momentum $l_c = r \times k$ (where r and k denote, respectively, the position and momentum vectors of the electron relative to the projectile core), an orbital quantum number l_1 is defined by the condition (Becker and MacKellar 1984):

$$l_1 \leqslant l_c \leqslant l_1 + 1 \tag{1}$$

Second, a classical number n_c is defined from the relation $E_c = -q^2/2n_c^2$, where q is the net charge of the ionic core, and E_c is the calculated classical binding energy of the electron relative to the projectile core. Then, from the integer value l_1 attributed to l_c and the classical value n_c, a principal quantum number n_1 is defined by the condition:

$$\left[\left(n_{l_1}^* - 1\right)\left(n_{l_1}^* - \tfrac{1}{2}\right)n_{l_1}^*\right]^{1/3} \leqslant n_c < \left[n_{l_1}^*\left(n_{l_1}^* + \tfrac{1}{2}\right)\left(n_{l_1}^* + 1\right)\right] \tag{2}$$

and the relation

$$n_{l_1}^* = n_1 - \delta(l_1). \tag{3}$$

Condition (2) is equivalent to that used in the case of fully stripped ion projectiles (Becker and MacKellar 1984) where the effective quantum number $n_{l_1}^*$ is replaced by n_1. If $l_1 < n_1$, the final nl-sublevel is defined by $n = n_1$ and $l = l_1$. If $l_1 \geqslant n_1$, the final

nl-sublevel is defined by $l = l_1 - 1$ and n determined from conditions (2) and (3), with l_1 replaced by l.

The binning procedure described here is not very different from that used for fully stripped ion projectiles (Olson *et al* 1992), in which a principal quantum number n is first determined from n_c and condition (2), and where the value of l is then defined from relation (1) with l_c replaced by the normalized classical momentum $(n/n_c)l_c$. The two binning procedures give very close results in the case of fully stripped ion projectiles.

We have verified that the normalization procedure used here for l_c occurs for less than 4% of the total number of trajectories ending at an electron capture process. Since in the present collisions the most populated levels are $n = 8$ and 9, the normalization procedure has no influence in the determination of the low-l sublevels, and only the largest values of l may be slightly affected. In our calculations, a large number of trajectories have been used to ensure final nl-distributions with small statistical errors, less than 3% for the most populated nl-sublevels.

The CTMC calculated nl-distributions are given in table 4 for projectile energies between 1.0 keV amu^{-1} and 4.0 keV amu^{-1}. The CTMC emission cross sections of experimentally observed lines are given in table 5 for the same projectile energies. There is a good agreement between the calculations and the measurements. This agreement confirms that the methods we have used to determine the experimental cross sections are not so bad. It confirms also our previous line identifications (Jacquet *et al* 1993).

Table 4. CTMC calculated cross sections (in 10^{-16} cm^2) versus the projectile energy (keV amu^{-1}) for single electron capture into the $8l$ and $9l$ sublevels for Ar^{8+}–Li collisions.

Energy nl	1.0	1.5	2.0	2.5	3.0	3.5	4.0
8s	28.17	27.03	23.32	17.77	14.34	11.26	8.85
8p	61.28	42.61	31.64	24.41	18.69	14.92	11.81
8d	19.81	14.88	11.26	8.45	7.42	6.29	5.54
8f	9.28	7.15	5.66	4.83	4.12	4.45	4.52
8g	13.29	11.98	11.34	11.15	11.35	11.58	10.93
8h	21.28	22.32	22.54	20.56	21.65	23.15	24.54
8i	34.55	35.80	34.54	36.29	37.03	39.98	41.97
8k	52.76	51.89	52.82	54.36	50.25	50.24	48.44
total	240 41	213.66	193.13	177.82	164.84	161.88	156.61
9s	33.81	23.36	13.98	9.13	5.37	3.44	2.18
9p	29.74	19.40	12.47	8.54	6.46	5.02	4.20
9d	12.40	9.55	7.66	5.78	4.92	4.17	3.86
9f	6.57	5.17	4.58	4.33	4.37	4.45	4.47
9g	10.46	11.15	10.92	11.57	11.24	9.69	9.03
9h	19.33	21.70	19.86	20.29	19.81	19.06	19.67
9i	29.65	32.27	32.10	32.62	36.48	40.06	43.46
9k	36.55	42.37	48.03	50.94	57.98	62.99	66.16
9l	26.08	42.92	60.75	66.73	67.81	67.01	64.46
total	204.58	207.88	210.39	209.94	214.44	215.90	217.48

The total cross section $\sigma(n)$ is larger for $n = 9$ than for $n = 8$ (cf tables 3 and 4), but the core-electron effect on the nl-distribution is more significant for $n = 8$ than for $n = 9$. This can be explained (Harel and Jouin 1988, Jacquet *et al* 1994) by contributions of non-adiabatic couplings involved in the population of the low l states which are more efficient when the energy splittings between adiabatic potential curves are larger. Both experiment

Table 5. CTMC calculated emission cross sections (10^{-16} cm^2) versus the projectile energy (keV amu^{-1}) for single electron capture following Ar^{8+}–Li collisions.

Energy transition	1.0	1.5	2.0	2.5	3.0	3.5	4.0
7p–8s	3.08	2.94	2.54	1.94	1.56	1.23	0.965
7d–8p	4.97	3.46	2.55	1.96	1.49	1.18	0.934
7d–8f	0.399	0.323	0.271	0.244	0.215	0.220	0.220
7f–8d	0.539	0.403	0.303	0.227	0.199	0.169	0.149
7f–8g	2.53	2.45	2.32	2.33	2.37	2.38	2.31
7g–8h	*10.11*	*10.84*	*10.93*	*10.66*	*11.66*	*12.56*	*13.42*
7h–8i	34.03	37.84	39.07	42.55	46.60	50.70	52.70
7i–8k	82.78	103.59	125.85	138.18	137.46	137.14	131.11
8p–9s	2.73	1.89	1.13	0.739	0.435	0.279	0.178
8d–9p	1.79	1.18	0.759	0.520	0.394	0.307	0.257
8d–9f	0.162	0.130	0.117	0.112	0.113	0.114	0.114
8f–9g	1.03	1.11	1.09	1.16	1.13	0.987	0.925
8g–9h	3.92	4.43	4.11	4.25	4.24	4.11	4.28
8h–9i	11.11	12.23	12.19	12.79	14.55	16.00	17.29
8i–9k	23.85	28.85	32.24	35.51	40.94	44.62	45.98
8k–9l	28.33	48.72	70.08	79.41	81.86	80.93	77.22
4d–4f	0.100	0.115	0.126	0.137	0.143	0.148	0.150
9h–10i	0.913	1.18	1.35	1.53	1.81	1.91	2.12
9i–10k	1.71	2.15	2.33	3.19	3.99	4.78	5.04
9k–10l	2.57	4.65	4.79	6.91	8.32	9.36	8.59
9l–10m	2.07	5.34	8.86	12.07	12.93	12.68	11.57
8g–10h	0.618	0.757	0.853	0.831	0.895	0.872	0.825
8h–10i	1.08	1.40	1.60	1.81	2.15	2.27	2.52
8i–10k	1.61	2.03	2.20	3.00	3.76	4.50	4.75
8k–10l	1.44	2.61	2.69	3.88	4.67	5.26	4.83
9h–11i	0.274	0.274	0.233	0.311	0.427	0.350	0.385
9i–11k	0.348	0.336	0.275	0.522	0.743	0.603	0.522
9k–11l	0.263	0.479	0.308	0.639	0.981	0.984	0.826
9l–11m	0.123	0.432	0.349	0.525	0.956	1.04	0.944

and theory show that the nl-distributions are not statistical: states with large l values are strongly populated, but also states with low l values ($l = 0, 1, 2$). They also show that the populations of the states of large angular momenta do not depend on the projectile energies in the studied energy range (figures 2(a) and (b)). The effect of the projectile core-electrons is strongly energy dependent: for a given nl-state ($n = 8, 9$ and $l = 0, 1, 2$), the $\sigma(nl)$ cross sections increase more or less strongly with decreasing energies (figures 3(a) and (b)), i.e. the effect of the projectile core-electrons increases with decreasing energies.

Following Harel and Jouin (1988), and as already discussed in the case of Kr^{8+}–Li(2s) collisions (Jacquet *et al* 1994), we may explain the dependence of the cross sections with the energy as the effect of successive avoided crossings between adiabatic potential energy curves which are correlated asymptotically to the Ar^{8+}–Li entrance channel and the various $Ar^{7+}(nl)$ + Li^+ outgoing channels. At high energies, the avoided crossings are nearly adiabatic: states with large l values are predominantly populated by the Stark effect of the residual ion. As the energy decreases, the non-adiabatic couplings at the avoided crossings become successively more and more efficient, beginning with those associated with the lowest $Ar^{7+}(nl)$ + Li^+ outgoing channels. This explains the increase of the cross sections as the energy decreases for the lowest l values (l = 0–3), while the cross sections for capture

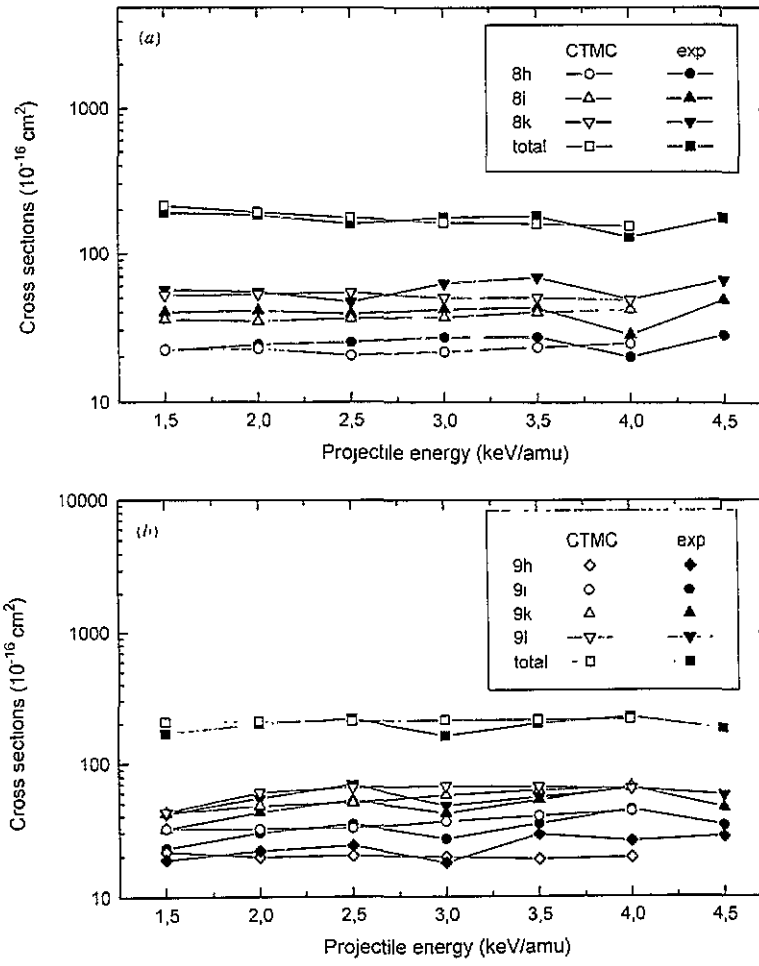

Figure 2. Experimental and CTMC cross sections $\sigma(n)$ and $\sigma(nl)$ with large l values versus the projectile energy between 1.5 keV amu^{-1} and 4.5 keV amu^{-1}. (a) $n = 8$. (b) $n = 9$. The lines have been drawn to help guide the eye.

into $l \geqslant 4$ remain nearly constant or decrease (in agreement with zero quantum defects for these sublevels).

As the energy decreases much more, the cross sections for the lowest l should go through a maximum since the non-adiabatic couplings should begin to decrease. Such a behaviour is indeed implicated by the CTMC calculated cross section for capture into the 8s sublevel (see table 4) and should be observed at much lower energies than investigated here for capture into the other lowest nl-sublevels ($l \simeq 1$–3).

However, at these low energies, the collisions are in the molecular regime, and the non-adiabatic couplings between different n levels may also contribute. This is indeed observed in the case of the calculated cross section for capture into the $n = 8$ level, which increases as the energy decreases (see table 4).

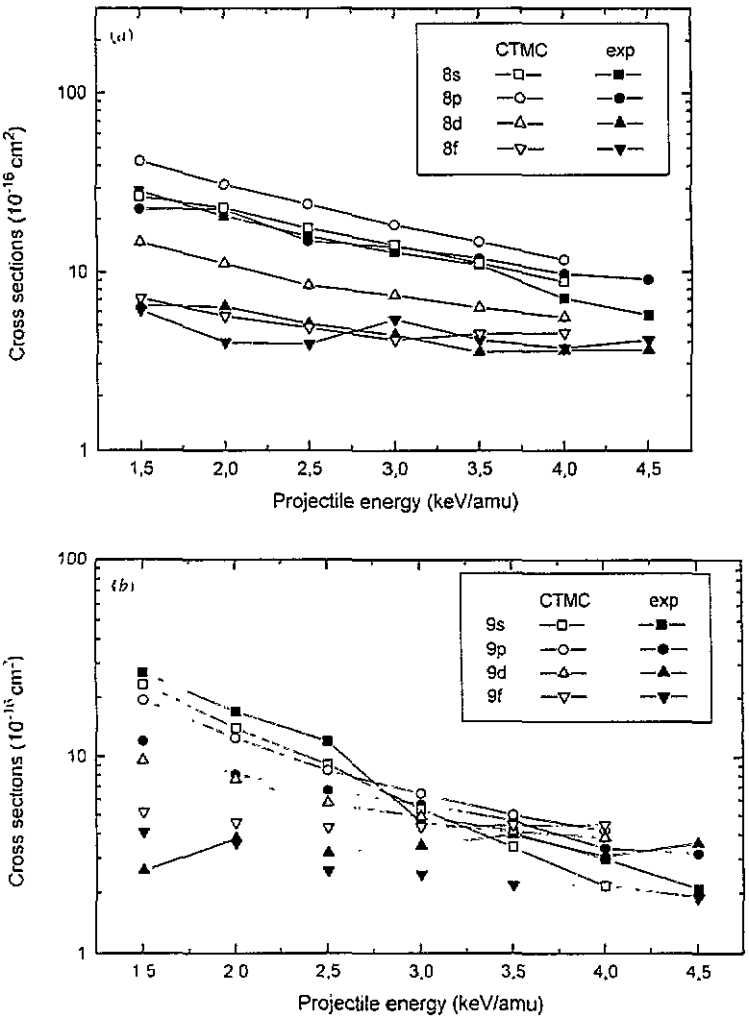

Figure 3. Experimental and CTMC cross sections $\sigma(nl)$ with low l values versus the projectile energy between 1.5 keV amu^{-1} and 4.5 keV amu^{-1}. (a) $n = 8$. (b) $n = 9$. The lines have been drawn to help guide the eye.

5. Conclusion

We have shown experimentally that the projectile core-electrons influence the final nl-distributions resulting from single electron capture following Ar^{8+}–Li collisions. This effect depends strongly on the projectile energy in the 1.5–4.5 keV amu^{-1} energy range as already predicted by CTMC calculations (Jacquet *et al* 1994). Similar effects are also predicted by CTMC calculations in the case of Kr^{8+}–Li collisions in the 1.5–15 keV amu^{-1} energy range: it would be interesting to study them. Indeed, for a given n state ($n = 8$, 9 and $l = 0$, 1, 2), the $\sigma(nl)$ cross sections increase more or less strongly with decreasing energies. The effect of the projectile core-electrons vanishes at high energies.

References

Abrines R and Percival I C 1966 *Proc. Phys. Soc.* **88** 861–72
Becker R C and MacKellar A D 1984 *J. Phys. B: At. Mol. Phys.* **17** 3923–42
Denis A, Martin S, Chen L and Désesquelles J 1994 *Phys. Rev.* A **50** 2263–8
Dijkkamp D, Brazuk A, Drentje A G, de Heer F J and Winter H 1984 *J. Phys. B: At. Mol. Phys.* **17** 4371–85
Gauntt D M and Danzmann K 1992 *Phys. Rev.* A **46** 5580–93
Harel C and Jouin H 1988 *J. Phys. B: At. Mol. Opt. Phys.* **21** 859–83
Jacquet E, Boduch P, Chantepie M, Druetta M, Hennecart D, Husson X, Lecler D, Martin-Brunetière, Olson R E, Pascale J and Wilson M 1994 *Phys. Scr.* **49** 154–65
Jacquet E, Boduch P, Chantepie M, Druetta M, Hennecart D, Husson X, Lecler D, Olson R E, Pascale J, Stolterfoht N and Wilson M 1993 *Phys. Scr.* **47** 618–27
Jacquet E and Pascale J 1995 *Nucl. Instrum. Methods* at press
Klapisch H 1967 *C. R. Acad. Sci., (Paris)* B **265** 914
Lindgård A and Nielsen S E 1977 *At. Data Nucl. Data Tables* **19** 563–633
Martin S, Denis A, Ouerdane Y, Carré M, Buchet-Poulizac M C and Désesquelles J 1992 *Phys. Rev.* A **46** 1316–20
Niehaus A 1986 *J. Phys. B: At. Mol. Phys.* **19** 2925–37
Olson R E, Pascale J and Hoekstra R 1992 *J. Phys. B: At. Mol. Opt. Phys.* **25** 4241–7
Olson R E and Salop A 1977 *Phys. Rev.* A **16** 531–41
Pascale J, Olson R E and Reinhold C O 1990 *Phys. Rev.* A **42** 5305–14
Reinhold C O and Falcon C A 1986 *Phys. Rev.* A **33** 3859–66
Theodosiou C E, Inokuti M and Manson S T 1986 *At. Data Nucl. Data Tables* **19** 473